Uptake and localisation of rhenium *fac*-tricarbonyl polypyridyls in fluorescent cell imaging experiments†

Vanesa Fernández-Moreira,‡[a] Flora L. Thorp-Greenwood,‡[a] Angelo J. Amoroso,[a] Joanne Cable,[b] Jonathan B. Court,[b] Victoria Gray,[b] Anthony J. Hayes,[c] Robert L. Jenkins,[a] Benson M. Kariuki,[a] David Lloyd,[b] Coralie O. Millet,[b] Catrin Ff. Williams[b] and Michael P. Coogan*[a]

Received 24th March 2010, Accepted 4th June 2010
First published as an Advance Article on the web 30th June 2010
DOI: 10.1039/c004610h

The synthesis of a series of rhenium *fac* tricarbonyl bisimine complexes and their application as lumophores in fluorescence imaging of yeast and human adenocarcinoma cells is reported. A wide range of complexes are synthesised with varying charges and lipophilicities, all of which have photophysical properties which make them suitable as cell imaging agents. After attempts to apply these as imaging agents in various strains of yeast which showed limited uptake, an investigation was undertaken of their applications as imaging agents in mammalian cells. In general the uptake was high and short-term toxicity and photobleaching appear to be low. The patterns of uptake and localisation are correlated with structural and electronic features of the complexes in an attempt to establish ground-rules for the design and application of rhenium complexes in imaging of eukaryotes.

Introduction

Since the advent of metallopharmaceuticals such as cisplatin the application of synthetic metal complexes, including radioisotopes, in diagnostic and therapeutic biomedical contexts has developed dramatically; however, the ground-rules appertaining to the uptake and transport of such species are far less clear than for either essential metal ions, or exogenous organic therapeutic and imaging agents.[1a,b] Many of the best known organic fluorophores commonly applied as imaging agents are planar or near planar,[2] and it is likely that there will be significant differences between their interactions with *e.g.* sheet-like phospholipid bilayers and those with more complex and sterically demanding geometry. A fuller understanding of how typical metalloagents such as octahedral transition metal complexes interact with biological membranes and behave in cellular environments will be necessary for many imaging and therapeutic applications. In particular, the application of d^6 metal complexes in fluorescent cell imaging is an emerging research area which has recently received a great deal of attention.[1c] The attractive intrinsic photophysical properties common to many Ir(III),[1d] Re(I)[1e] and Ru(II)[1f] complexes, such as large Stokes shifts, long luminescence lifetimes and resistance to photobleaching, make these excellent candidates for applications in cell imaging. Large Stokes shifts are useful in fluorescence imaging as autofluorescence from endogenous fluorophores, *e.g.* NAD(P)H, flavin or chlorophyll, can be confused with desired lumophore emission (NB although rhenium complexes commonly display phosphorescence, and the technique is described as fluorescence microscopy, the term lumophore is used throughout to avoid differentiating between mechanisms of emission).[2] Typically, autofluorescence Stokes shifts are small (tens of nm) and large Stokes shift lumophores allow autofluorescence to be eliminated without losing signal intensity. Similarly, luminescence lifetime can be used to filter out short-lived autofluorescence when a lumophore has a significantly longer lifetime.[2] Photobleaching usually occurs when the excited state of a lumophore reacts with oxygen species (sometimes autogenous photoproducts) giving non-emissive products. Rapid destruction of lumophores upon intracellular irradiation then leads to loss of signal intensity and can seriously compromise time-resolved studies of cellular processes.[2] However, while there are now a number of examples of individual d^6 complexes applied in cell imaging, as yet the basic rules for the uptake and localisation of each family of complexes are only just beginning to emerge.[1] Much of the focus with Ru complexes has concerned the use of complexes of highly conjugated aromatic ligands designed to act as intercalators for DNA/RNA especially for demonstration of nuclear localisation.[3] There have been studies of Ir and Re species bearing specific chemical groups designed to interact with particular biological entities,[4] but as yet there is no general study of the uptake and localisation of a range of complexes of these metals. In comparison, the rules relating to the patterns of localisation of certain families of lanthanide-based lumophores are better understood and have been more extensively studied.[5] Previous reports of the application of rhenium complexes in cell imaging fall into two distinctive patterns. This group has previously reported the application of a small range of rhenium complexes of relatively simple structure in a parasitic flagellate, *Spironucleus vortens*, as a preliminary investigation into their uptake and localisation.[6] Other reports, both from this group and others, have involved the imaging of mammalian cells (usually human carcinoma cells, either HeLa or MCF-7) and the imaging agents have been highly

[a]*School of Chemistry, Cardiff University, Cardiff, Wales, UK CF10 3AT. E-mail: cooganmp@cf.ac.uk; Fax: (+) 4402920874030*
[b]*School of Biosciences, Cardiff University, Cardiff, Wales, UK CF10 3AT*
[c]*Confocal Microscopy Unit, Cardiff School of Biosciences, Life Sciences Building, Cardiff, Wales, UK CF10 3US*

† Electronic supplementary information (ESI) available: X-Ray crystallographic data for **14** and **15**. See DOI: 10.1039/c004610h

‡ Equal contribution from these authors.

specialised, and usually very complex. To date, rhenium complexes conjugated to fMLF (a small peptide used as a targeting agent for formyl peptide receptor, FPR),[7] biotin[8] and cobalamine[9] have been applied in cell imaging, as has a chloromethyl rhenium complex designed to target mitochondria,[10] and a dipicolylamine rhenium derivative which responds to zinc ions.[11] There has not, however, been a systematic investigation of the uptake and localisation properties intrinsic to the rhenium tricarbonyl skeleton to inform the design of future imaging agents. Here, we report the results of a more systematic qualitative study of the patterns of uptake and localisation of a series of rhenium tricarbonyl bisimine complexes of varying lipophilicity, charge, size and structural type in yeast and in human adenocarcenoma MCF-7 cells.

Results and discussion

Design and synthesis of complexes

The standard methods for the preparation of luminescent rhenium tricarbonyl species are typically to react the commercially available rhenium pentacarbonyl halides with a bisimine ligand such as bipyridine or phenanthroline.[10] These reactions typically give stable rhenium bisimine *fac*-tricarbonyl halides which require further activation in order to allow coordination of the axial pyridine derivative. There are a variety of methods available for this activation, the three most common being: i) halide abstraction with silver salts in the presence of a pyridine can lead directly to the cationic pyridine derivative; ii) halide abstraction in acetonitrile to give the (usually) cationic and highly labile acetonitrile complex; iii) conversion of the halide to the triflate by treatment with triflic acid, being the most commonly encountered three approaches. In the latter two cases the activated complexes are then treated with the desired pyridine derivatives (usually in THF) to give the final species. As the bisimine ligand is the one involved in the MLCT process[12,13] it was decided to use the axial ligand in order to incorporate groups which tune the solubility, lipophilicity *etc.* of the complex without (usually) affecting the photophysical properties. Conjugation of simple pyridines in the axial position of the complexes to alkyl chains and rings was selected to tune the lipophilicity of the agents. While it is more usual to perform coupling reactions on free ligands, post-coordination modification of ligands has previously proved useful in the synthesis of rhenium complexes for use in cell imaging, and as part of this investigation two approaches to the systems required were investigated: coordination of simple pyridines followed by coupling reactions of the complex and synthesis of the conjugated ligands followed by coordination. Interestingly, it will be seen that the preferred approach varies with the overall charge of the complexes.

Cationic complexes

In order to provide mutually comparable results it was decided that the polypyridyl portion of the complex should be represented in each cationic case by bipyridine, and the axial pyridine ligand should be varied through a series of functional group variations in the 3-position. Thus, rhenium tricarbonyl bipyridine halides were prepared by reaction of bipyridine with the rhenium pentacarbonyl halides. Direct reaction of these halo-species with pyridine and hydroxymethyl pyridine, respectively, in the presence of silver tetrafluoroborate gave the complexes **1**[12] and **2**[6] in good yields (Scheme 1). For more complex species the halides were activated as the triflate **3** or acetonitrile derivative **4** as previously discussed (Scheme 2).

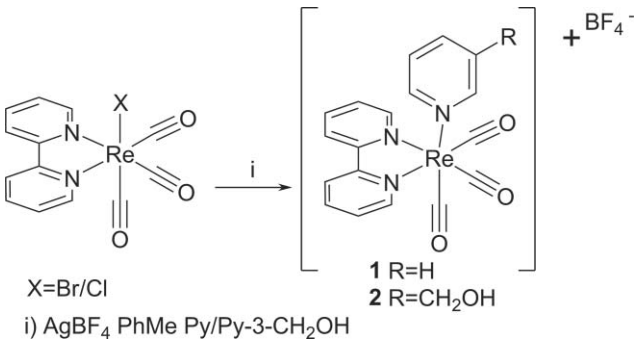

Scheme 1 Synthesis of simple $Re(CO)_3(bipy)(Py_X)$ complexes

A series of non-commercially available pyridyl ligands of varying lipophilicities and structures were prepared by simple organic transformations. As it was of interest to compare lipophilic species of different structures, alkyl chains and cyclohexyl rings were incorporated into the ligands. As there are cases in which esters have been known to break down in the cellular environment[14] an amide bearing a lipophilic group was also prepared (derived from cyclohexylamine). The alkyl chain-containing complexes were derived from fatty acids conjugated to a hydroxyl-substituted pyridine, while the cyclohexyl rings were incorporated as the ester and amide derived from cyclohexanol[15] and cyclohexylamine,[16] respectively, and nicotinic acid. In all cases two approaches to the

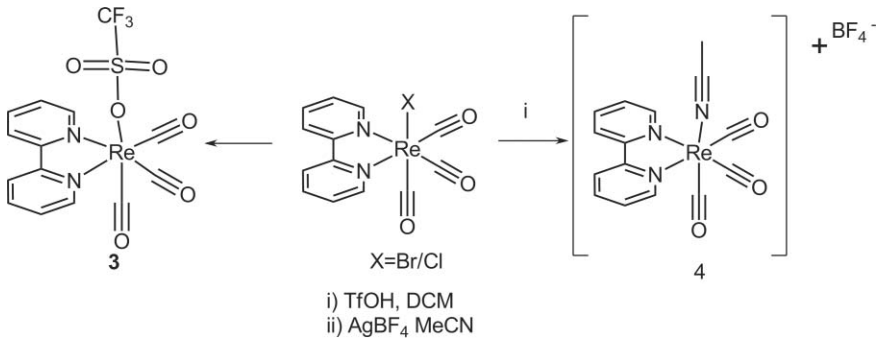

Scheme 2 Activation of rhenium complexes by halide loss.

complexes were attempted, namely pre-formation of the lipophilic ligand followed by coordination to rhenium, and the conjugation of a preformed rhenium complex to the lipophilic component. Coupling of 3-hydroxymethylpyridine with a variety of fatty acids using EDCI gave the derived esters, **5–7**[6] (Scheme 3) which were then reacted with **4** to give a series of complexes **8–10** bearing differing chain length fatty acids (Scheme 4). The analogous coupling reactions of the pre-coordinated species **2** with the relevant fatty acids gave the complexes **8–10** but in lower overall yields than the alternative route in which the pyridine and fatty acid were pre-conjugated (Scheme 5).

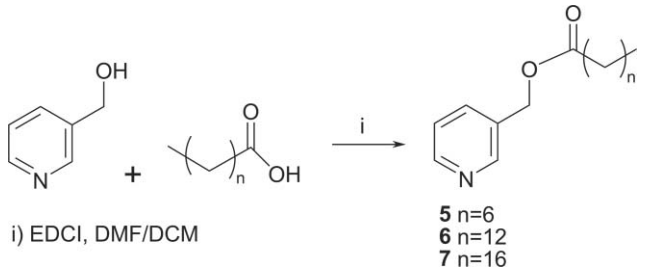

Scheme 3 Synthesis of fatty-acid-derived pyridine ligands.

Reaction of nicotinic acid chloride **11**[17] with cyclohexanol and cyclohexylamine gave the analogous ester **12** and amide **13**. These cyclohexyl ligands were then reacted with rhenium bipyridyl acetonitrile complex **4** to give the derived cationic complexes **14** and **15**, respectively (Scheme 6). Again, the attempted conjugation of the nicotinic acid complex **16**[18] with cyclohexylamine and cyclohexanol proved less successful than the more traditional

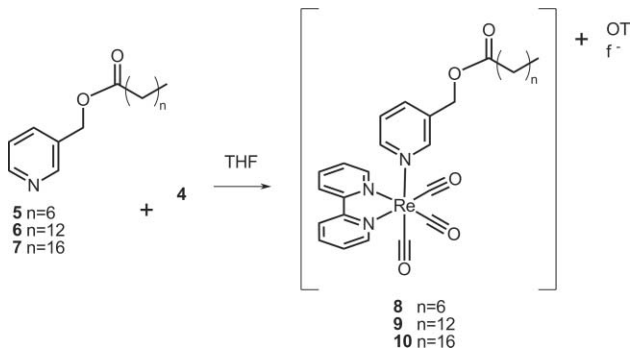

Scheme 4 Synthesis of lipophilic rhenium complexes from pre-coupled ligands.

approach, giving very poor yields of the required species after complex isolation procedures (Scheme 7).

These cyclohexyl species were more crystalline than the fatty acid derivatives **8–10** and crystals for X-ray diffraction[19] were grown of **15**; however, the crystals of the cyclohexanol-derived species **14** were of poor quality and while various diffraction data sets were obtained which could be solved, a satisfactory refinement could not be achieved. The analogous amide **15** gave a well resolved structure in space group $P21/c$. The structure showed essentially octahedral geometry and confirmed the expected *fac* disposition of the carbonyl ligands (Fig. 1). The bond lengths and angles were again within the range expected for analogous complexes and the deviation from ideal octahedral geometry (average $N_{(Py)}$–Re–$N_{(bipy)}$ angle = 83.7°) can be explained by crystal packing forces (Fig. 2). Crystal packing is dominated by interactions between

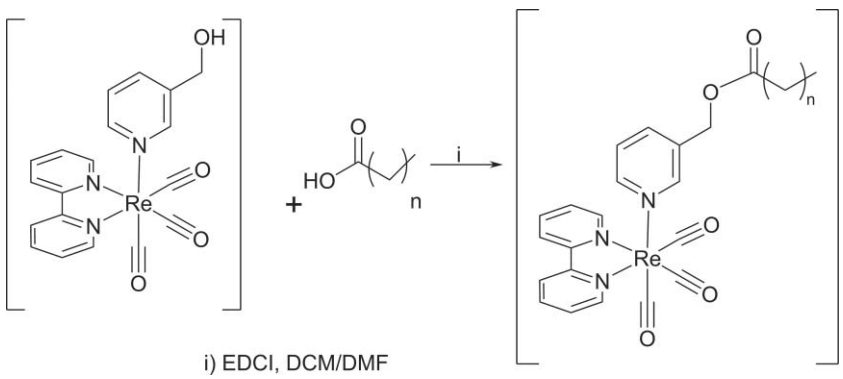

Scheme 5 Synthesis of lipophilic rhenium complexes by post-coordination modification.

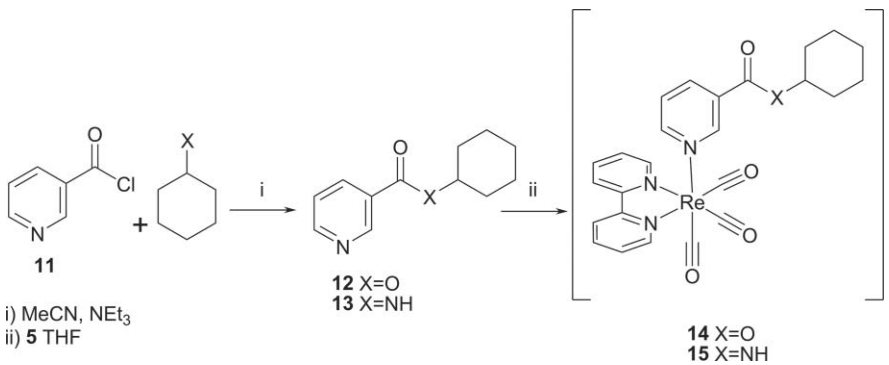

Scheme 6 Synthesis, and coordination of cyclohexyl pyridine ligands.

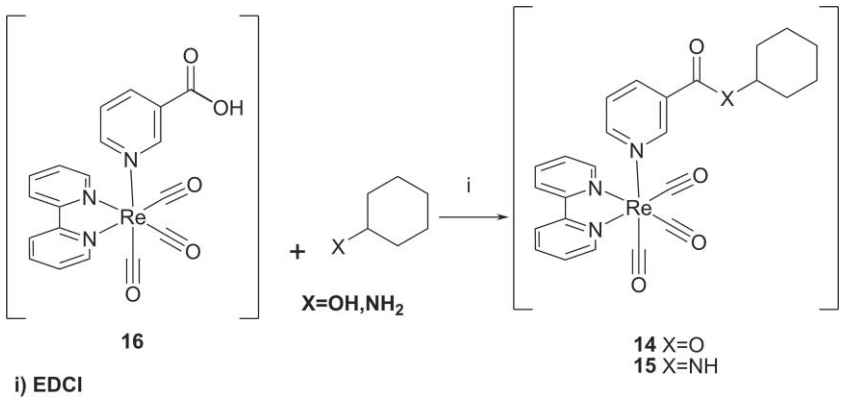

Scheme 7 Synthesis of cyclohexyl complexes by post-coordination modification.

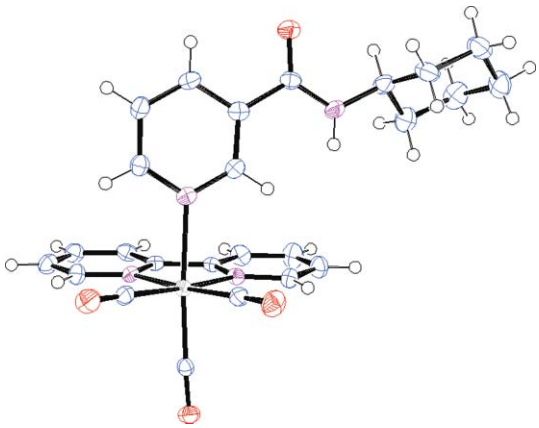

Fig. 1 ORTEP[20] image of asymmetric unit of **15** (50% probability).

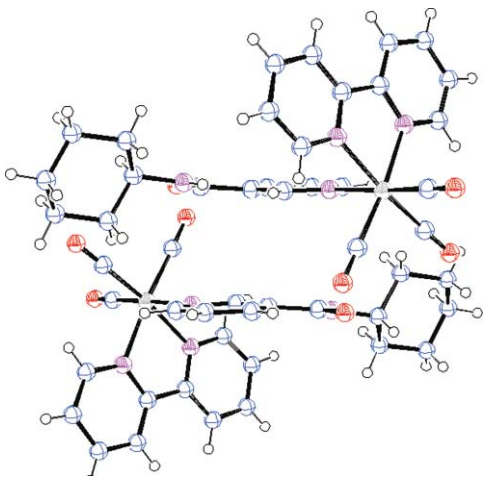

Fig. 2 ORTEP[20] image of packing of **15** (50% probability).

the cyclohexyl rings and the bipyridines, leading to the <90° angle observed between these groups. However, an additional interaction between the nicotinamide units leads to a close interaction (<3.5 Å) between these π-systems (Fig. 2). Full details of refinement and structure, and tables of selected bond angles and lengths are included in the supplementary information.† The relative lipophilicities of these species are indicated by the log $P_{o/w}$ which were measured for a simple cationic complex **2**, log $P_{o/w}$ = –0.37, and the myristryl derived species **9**, log $P_{o/w}$ = 0.91.

Anionic complexes

As a range of complexes of varying overall charge was desired, anionic ligands which could compensate for the cationic Re(I) centre were required. We have previously reported the synthesis of a small number of rhenium complexes derived from the anionic ligand bathophenanthroline disulfonic acid, which is commercially available as the sodium salt. However, in order to synthesise a larger range of complexes derived from this ligand a new synthetic method was required to overcome the difficulty of handling these species in non-aqueous solution, as it was rapidly realised that the rhenium halides derived from this ligand are highly susceptible to hydrolysis. Reaction of bathocuprine disulfonic acid sodium salt with rhenium pentacarbonyl chloride or bromide in acetonitrile gave the expected complex **17**. However, this anionic complex was of such low solubility in organic solvents that characterisation was only possible as a solution in water, and it was observed that upon standing in D_2O solution the complex suffered hydrolysis to the aqua species, **18**, which proved to be unreactive towards the pyridine ligands required. For this reason a counterion exchange process was performed on the ligand prior to coordination. The commercial disodium salt was treated with two equivalents of tetrabutylammonium hydrogen sulfate in water which resulted in the immediate precipitation of a jelly-like substance, assumed to be the organic electrolyte **19**. After an extraction into DCM and drying the product, **19** was isolated from the organic phase as an easily handleable, pale pink amorphous solid (Scheme 9). The use of the tetrabutylammonium salt **19** allowed the formation of soluble, anionic rhenium complexes which could be handled in organic solvents, thus avoiding problems of hydrolysis, which was problematical for **17** (Scheme 8). Reaction with rhenium pentacarbonyl chloride gave the expected tricarbonyl complex **20** in good yield (Scheme 10). The activated rhenium complex **21** was synthesised by stirring the anionic complex with triflic acid in DCM, and rapid substitution of the halide was observed (Scheme 11). With this activated complex **21** in hand, substitution of the axial ligand was attempted by heating with pyridine and with 3-hydroxymethylpyridine in polar solvents (Scheme 12). While in each case the desired products **22** and **23**, respectively, were obtained successfully, prolonged reaction times (5–7 days) were

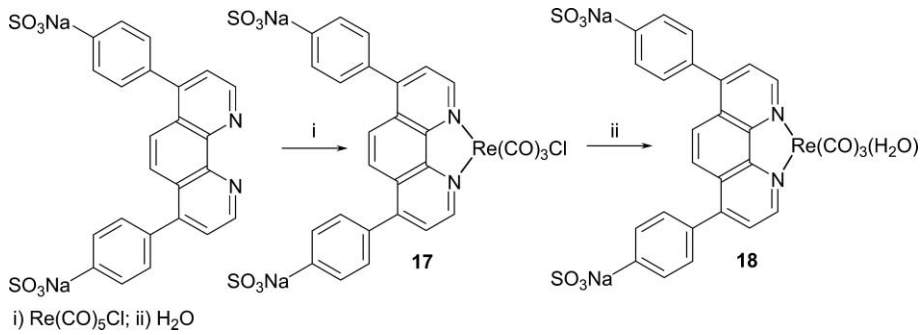

Scheme 8 Hydrolysis of water-soluble complexes.

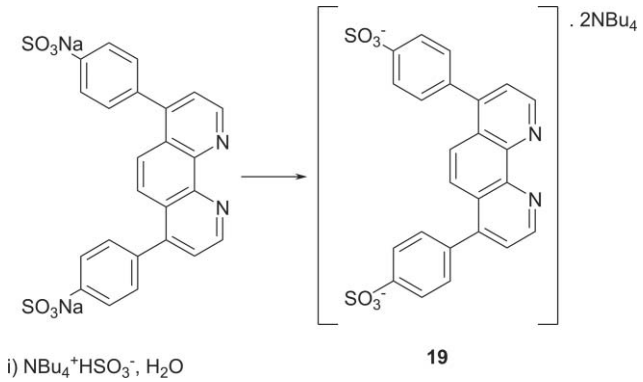

Scheme 9 Ion exchange to lipophilic sulfonated ligand.

required. It is postulated that these extended reaction times are due to the presence of sulfonic acids in the reaction mixtures derived from protonation of the ligand by triflic acid to the neutral complex **24** or the cationic species **25** (Scheme 13). Either of these species could protonate the potential ligands and thus lead to the prolonged reaction times, even in the presence of an excess of the pyridine, by lowering the nucleophilicity of the nitrogen by hydrogen bonding. In order to avoid this complication, activation as the acetonitrile derivative **26** was attempted by halide abstraction with silver tetrafluoroborate in acetonitrile (Scheme 14) and the new activated rhenium complex **26** substituted with pyridine ligands (Scheme 15). In an attempt to demonstrate the possibility of further functionalisation of the complexes once a pyridine derivative was coordinated, the hydroxymethyl complex **27** was reacted with myristic acid in the presence of EDCI and DMAP in DCM, giving a much more lipophilic complex **28** than those previously synthesised. Interestingly, in this case precoordination of 3-hydroxymethyl pyridine followed by post-coordination modification proved the more effective approach (Scheme 16). After having synthesised a variety of sulfonated rhenium complexes as tetrabutylammonium salts, the recovery of the water solubility was then achieved using ion exchange chromatography with Amberlite IR 120-H, as the ammonium form. Thus, three monoanionic complexes of varying lipophilicity have been prepared, each based around the rhenium *fac*-tricarbonyl bathophenanthroline disulfonate core, with axial ligands represented by pyridine, 3-hydroxymethylpyridine and 3-tetradecanoyloxypyridine, the latter being a lipophilic anionic species. In addition to the cationic species synthesised above, and the chloromethyl species **29** prepared from **2** (Scheme 17), this gave a range of species of varying lipophilicities, charges and reactivities. The simple anionic species are less lipophilic than the cations, with the simple pyridyl species **22** having log $P_{o/w} = -0.53$.

Photophysical characteristics of imaging agents

As the polypyridyl ligand involved in the MLCT luminescence was not varied throughout each of the series, with the cationic species containing a bipyridyl ligand and the anionic complexes a bathophenantholine disulfonate, the photophysics of the compounds were essentially identical for each series. The cationic

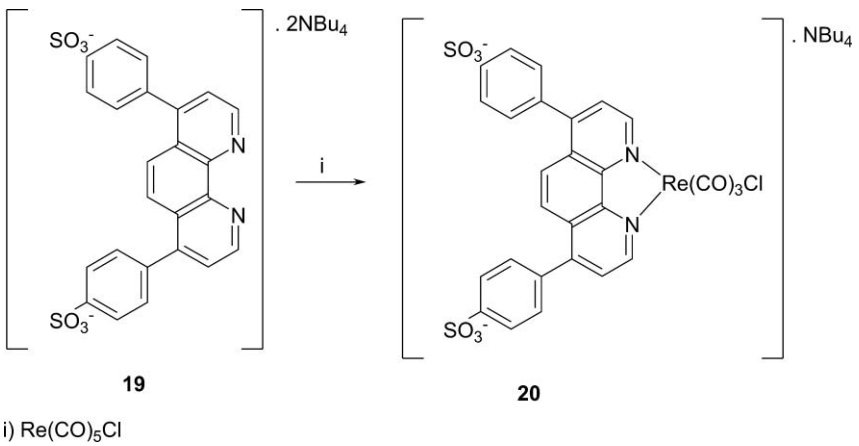

Scheme 10 Coordination of lipophilic sulfonated ligand.

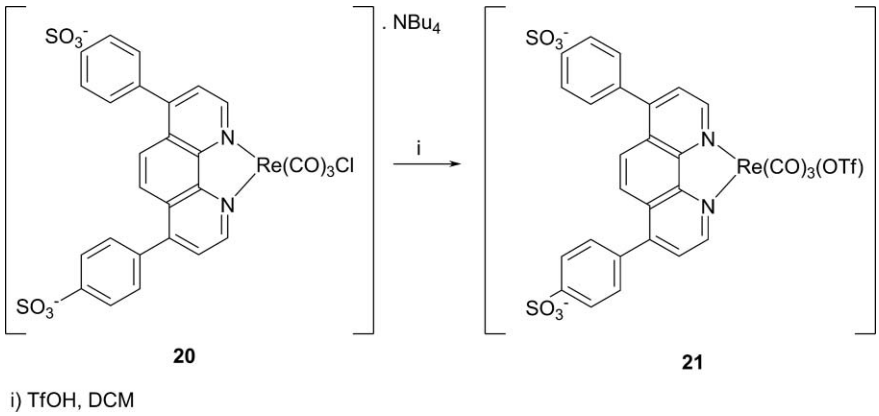

Scheme 11 Activation of anionic rhenium complex as triflate.

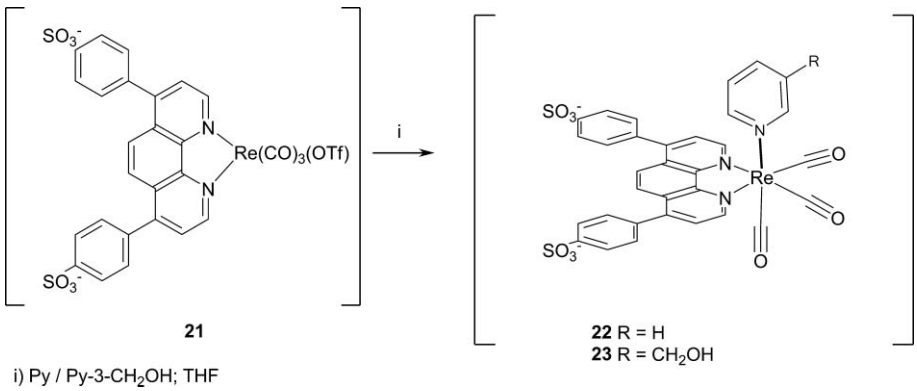

Scheme 12 Coordination of pyridines to activated anionic rhenium complex.

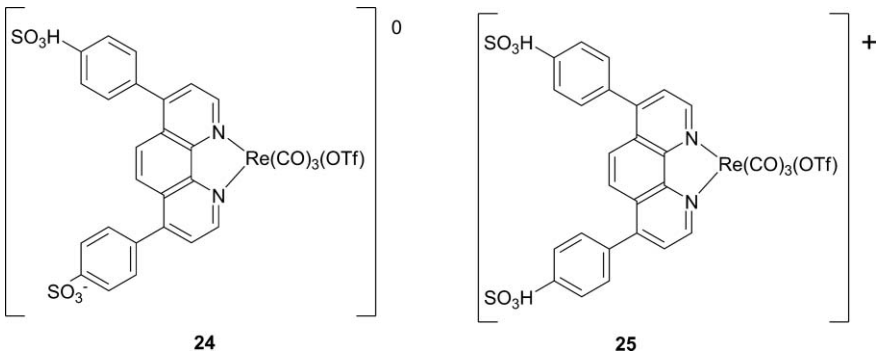

Scheme 13 Protonated forms of sulfated rhenium complexes.

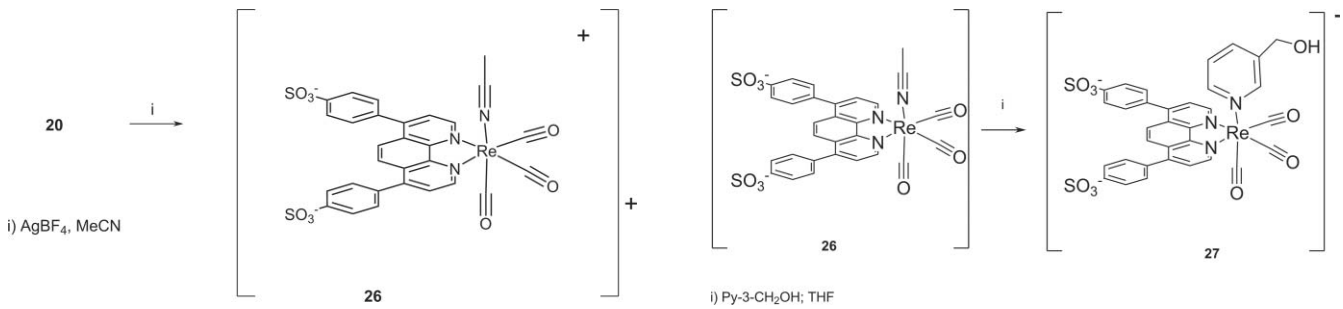

Scheme 14 Activation of sulfated rhenium complex as the acetonitrile adduct.

Scheme 15 Formation of hydroxymethyl rhenium complex **27**.

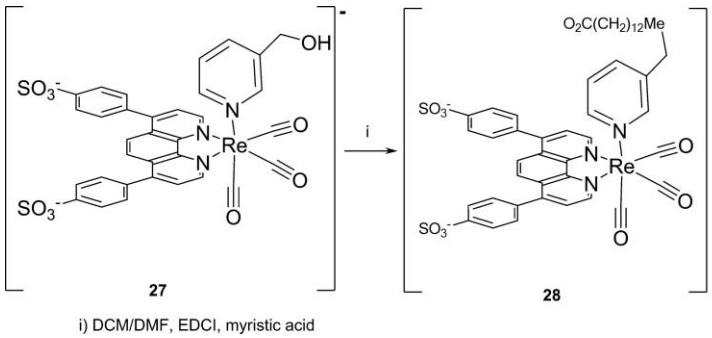

Scheme 16 Post-coordination modification of anionic rhenium complex **27**.

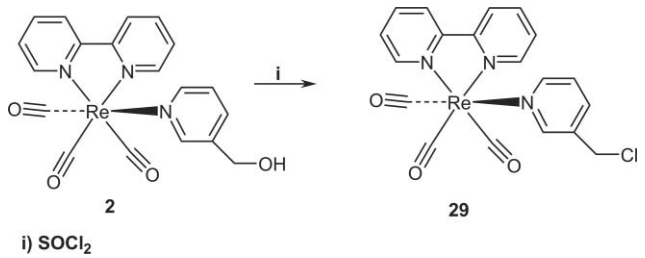

Scheme 17 Preparation of **29** according to ref. 10

species (Fig. 3) show broad featureless excitation and emission maxima at 380 and 550 nm, respectively, and the anionic species at 380 and 560 nm (Fig. 4). The excitation bands were assigned as ^{1}MLCT and the emission bands as ^{3}MLCT by comparison with previous studies. As the aim of this work was to investigate uptake and localisation of the species an in-depth study of the photophysical properties of the complexes (variable temperature measurements, time-dependent studies) was not undertaken, but the characteristics important for fluorescence microscopy applications (λ_{max} excitation, λ_{max} emission) are summarised in the supplementary information.† While the excitation maxima of all the species lies in the UV region of the electromagnetic spectrum, importantly the nature of the ^{1}MLCT excitation band, which is very broad, allows sufficient absorption in the visible region to allow the use of a 405 nm laser as the excitation source. It is important for cell imaging purposes to avoid UV excitation as UV has poor tissue penetration and also causes tissue damage. It is also convenient that many commercial fluorescence microscopes have an option for 405 nm excitation in confocal mode, and the poor excitation of TMRE at this wavelength (Fig. 5) allows differential excitation of the complexes in co-localisation experiments. The large Stokes shifts of all the species studied (150–200 nm) allows easy differentiation between emission emanating from the rhenium complexes and autofluorescence.

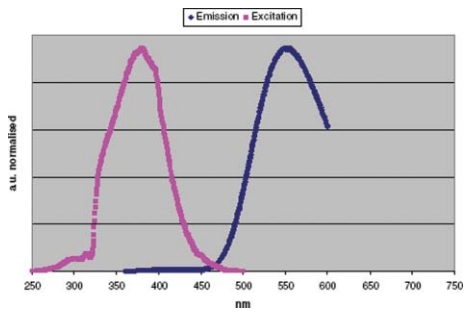

Fig. 3 Excitation and emission spectra of **14**.

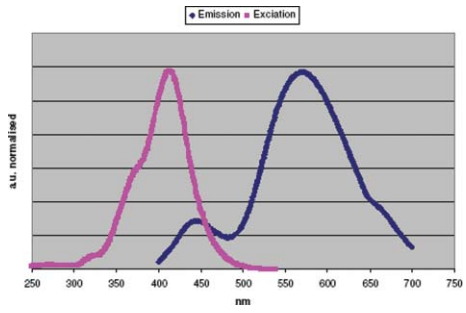

Fig. 4 Excitation and emission spectra of **27**.

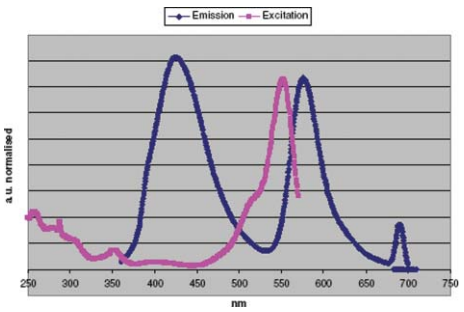

Fig. 5 Excitation and emission spectra of TMRE (note minimal excitation at 405 nm).

Cellular studies and confocal microscopy

Imaging experiments in yeasts

In order to establish ground-rules relating to the uptake and localisation of rhenium complexes by eukaryotic cells, an initial investigation of their uptake into yeasts (*Saccharomyces cerevisiae*) was undertaken. The results of these investigations were disappointing, in that across a variety of complexes both cationic and anionic, and with a range of lipophilicities, only a small proportion of the cells showed any detectable uptake of the lumophores (Fig. 6). The best uptake was seen with the cationic lipophilic species **9**, but even with this species only some of the population showed appreciable rhenium-based luminescence. Some uptake was also observed even for the anionic species (although less than in cationic species) and it appeared that the cells which showed uptake could be those which were in the process of budding, suggesting that the relatively impermeable cell wall associated with yeasts was preventing uptake, and it was only those in which the cell wall-membrane complex, involved in cellular proliferation-related activities, was imperfect which were taking in the lumophores (this pattern was also observed, although to a lesser extent, for the cationic species **9**, **29**) (Fig. 7). In order to probe the hypothesis that uptake of rhenium species was associated with division of yeast cells, further investigations were undertaken with fission yeast, *Schizosaccharomyces pombe*.[21] In this species, which typically grows to become a 14×3.5 μm cylinder and then divides transversely upon reaching this length, it follows that in a healthy growing and dividing sample there should be a correlation between

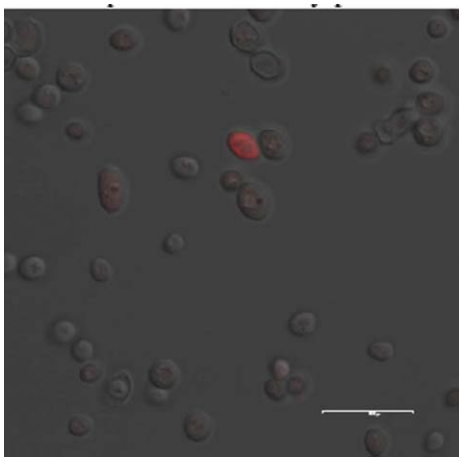

Fig. 6 Overlaid fluorescence and transmitted light images of **8** in *Saccharomyces cerevisiae* showing low uptake (scale bar = 15 μm).

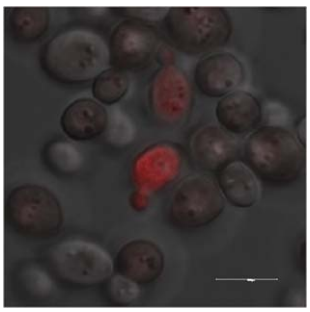

Fig. 7 Overlaid fluorescence and transmitted light images of **23** in *Saccharomyces cerevisiae* showing fluorescence concentrated in budding cells (scale bar = 6 μm).

length of a given cell and the stage of the division cycle. If, as had been hypothesised from the observations with *Saccharomyces cerevisiae*, uptake of lumophore is associated with a weakening of the cell boundary at a certain stage of division, then the intensity of luminescence should be a function of the stage of the division cycle and thus the length. Again, the lipophilic species **9** showed the best uptake (Fig. 8), but there was significant uptake for all species tested, including the anionic cases (Fig. 9). Unfortunately while the most intense luminescence did appear to be in small cells (*i.e.* those which had recently divided) there were also significant

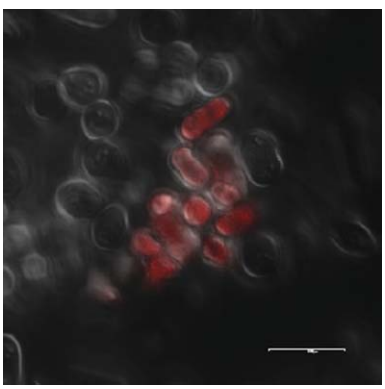

Fig. 8 Overlaid fluorescence and transmitted light images of **9** in fission yeast (scale bar = 8 μm).

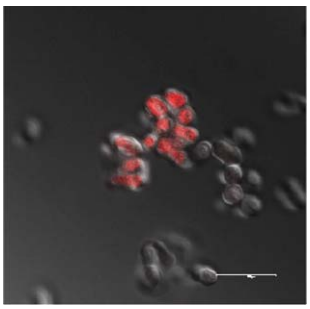

Fig. 9 Overlaid fluorescence and transmitted light images of **22** in fission yeast (scale bar = 12 μm).

numbers of the lengthier cells showing intense luminescence, so it was not possible to unambiguously correlate uptake with length, and therefore with stage of the division cycle. Again, as for bakers yeast, however, the majority of the sample of any length showed no luminescence, and so the level of uptake is low, and the mechanism of uptake remains ambiguous. While there appeared to be some interesting patterns of uptake and localisation of rhenium species in yeasts, it was felt that further study of systems in which such low levels of uptake was observed was not worthwhile. Therefore, attention turned to mammalian cells which have less impervious limiting layers. Thus, each of the species described above was incubated with MCF-7 (human adenocarcinoma) cells at a low temperature (4 °C) at which endocytosis is essentially inoperative.[2] This temperature was chosen so that the ability of the lumophores to permeate cells by passive diffusion could be assessed. It is important for lumophores not to be entrained in endosomes if they are to be capable of localising in *e.g.* mitochondria or nucleoli, and thus a non-endocytotic uptake mechanism was desirable. While the imaging experiments themselves were carried out at ambient temperature, the fluorophore-containing medium had been washed away by this point so re-emergence of endocytosis should not have interfered. It has previously been noted[8] for related complexes that both endocytosis and passive mechanisms can be at play in mammalian cells, so the low temperature was chosen in order to eliminate entrainment in endosomes which could give a misleading picture of the preferred sites of localisation.

Cationic complexes in MCF-7

Uptake of the cationic lipophilic complexes **8–10** bearing alkyl chains in MCF-7 cells was good to excellent with consistent patterns of uptake and localisation being observed. Liposome studies[6] had already indicated that these species were highly membrane permeable and therefore a high degree of cellular uptake had been expected. There were, however, several positive features to the observed uptake. Firstly, in no case was significant toxicity over the lifetime of the experiment observed, with normal cell structural morphology being maintained as well as it was in parallel experiments using known fluorophores of low toxicity such as TMRE; visual inspection indicated healthy cell morphology in >90% of cells in each sample. As a semi-quantitative test of toxicity MCF-7 cells were co-incubated with Trypan blue, which is only taken up by dead or dying cells, and a small number of complexes. Cell counts showed that Trypan blue had not been taken up by a greater number of cells in the samples treated with anionic species, (normalised to untreated blanks). However, the

cationic highly lipophilic species **9** showed relatively high toxicity at high concentrations, with as low as *ca.* 25% cell viability at 100μg ml^{-1} (normalised to untreated blanks). Presumably this is a result of membrane perturbation as previously noted in parasites.[6] Secondly, it was apparent that species **8–10** showed differing patterns of localisation. This was particularity gratifying as it had been suspected that the integrity of the ester linkages could be compromised within the cells by enzymatic hydrolysis. However, as hydrolysis by esterases would yield **2** in each case and the pattern of localisation of **8–10** were notably different (and in each case different from that observed for **2**) this was clearly not a significant problem. Localisation of **8–10** was observed in the cytoplasmic membrane and cytoplasm, with the cytoplasmic patterns being non-uniform, indicating localisation at lipophilic sites in organellar membranes, endoplasmic reticulum and the Golgi apparatus. The longer the chain the more specifically localisation was observed in the membranes, with **10** being essentially a membrane stain, and **8** and **9** more general cytoplasm (Fig. 10) and internal membrane targeting agents. A small degree of nuclear staining was observed with **9** with a highly specific pattern that appeared to indicate localisation in the nucleolus (Fig. 11); however, the small number of cells per sample showing this phenomenon made co-localisation to confirm this impractical. As the long-chain appended complexes could in principle act as surfactants and render membranes permeable, as a semi-quantitative test of permeability, MCF-7 cells were co-incubated with propidium iodide, which is only taken up when membranes are damaged or rendered permeable by surfactant, along with complexes **27** and **9**. Cell counts compared to untreated blanks showed that propidium iodide had not been taken up by a greater number of cells in the samples treated with anionic complex **27**; however, again complex **9** clearly shows perturbation of membranes with *ca.* 50% of cells above standards showing uptake. In order to eliminate the possibility that **8–10** were in fact hydrolysing to give **2**, the pattern of localisation of **2** was examined. Somewhat surprisingly **2** showed a pattern of localisation reminiscent of the mitochondrial localisation previously reported for the chloromethyl-substituted complex **29** (Fig. 12 and 13). This pattern of localisation has been confirmed by co-localisation experiments with TMRE and, in the case of **29**, had been attributed to the cationic lipophilic nature of the complex leading to a propensity for accumulation in mitochondria; thiol reactivity associated with the chloromethyl unit 'fixes' the lumophore in the mitochondria by irreversible reaction with *e.g.* GSH.

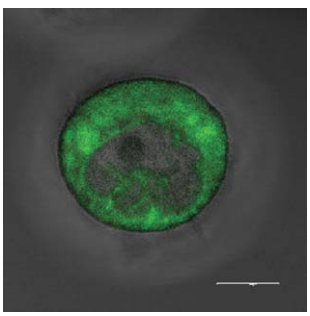

Fig. 10 Overlaid fluorescence and transmitted light images of **8** in MCF-7 cells showing localisation in the perinuclear cytoplasm (scale bar = 6 μm).

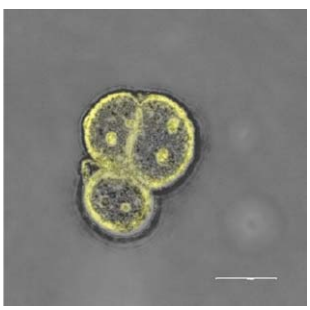

Fig. 11 Overlaid fluorescence and transmitted light images of **9** in MCF-7 cells showing nuclear localisation (scale bar = 12 μm).

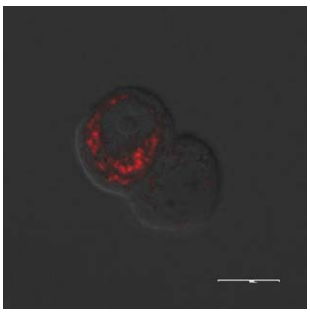

Fig. 12 Overlaid fluorescence and transmitted light images of 29 in MCF-7 cells showing mitochondrial localisation (scale bar = 14 μm).

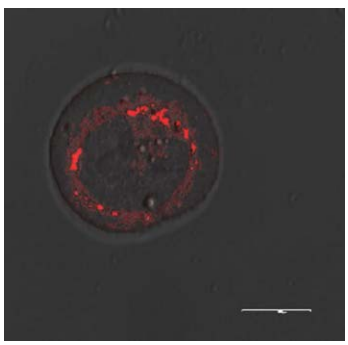

Fig. 13 Overlaid fluorescence and transmitted light images of **2** in MCF-7 cells showing mitochondrial localisation (scale bar = 9 μm).

That **2** shows such specific mitochondrial localisation (while other cationic lipopophilic complexes do not, *vide infra*/*supra*) suggests that **2** may also show thiol reactivity. While **2** lacks the chloromethyl group which is assumed to be the thiol-reactive unit of **29**, it is postulated that phosphorylation of the hydroxyl unit of **2** to give **30** confers thiol reactivity (Scheme 18), although it should be stressed that no evidence was obtained to support this hypothesis. A simpler cationic lipophilic complex which lacks the possibility for phosphorylation of **2** (and thus the ability to acquire thiol reactivity) is offered by the cyclohexyl ester **14**. The localisation of this species was more comparable to that observed for the fatty-acid-derived species **8–10**, showing non-uniform localisation in the cytoplasm, with little nuclear uptake but apparent localisation in organelles in the perinuclear region (Fig. 14). As it was of interest to compare this species with the chloromethyl species **29** (which is known to be thiol reactive) and the hydroxymethyl species which is thought to be phosphorylated

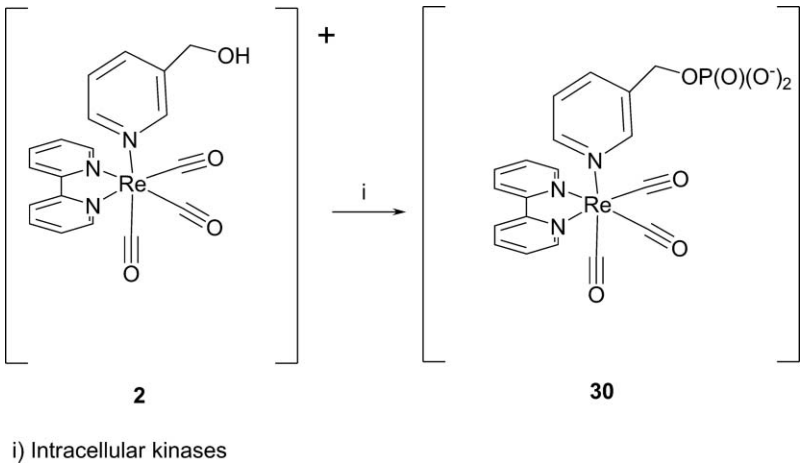

Scheme 18 Proposed activation of **2** by phosphorylation.

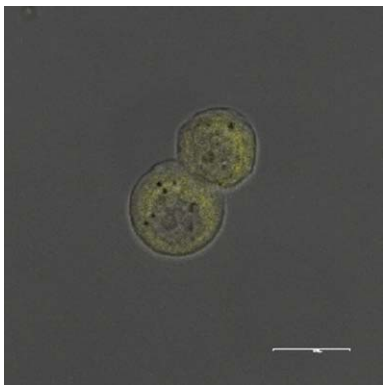

Fig. 14 Overlaid fluorescence and transmitted light images of **14** in MCF-7 cells (scale bar = 14 μm).

and also accumulates in mitochondria, similar colocalisation experiments were performed with **14** and TMRE to assess the importance of thiol reactivity in the localisation of these species.

The colocalisation experiments (Fig. 15 and 16) demonstrated that while some of the species had colocalised, indicating that **14** is present in mitochondria, its distribution was far more widespread and diffuse than that of TMRE. In comparison to the thiol reactive species **2** and **29**, the distribution of **14** in the cells was again more diffuse, supporting the theory that thiol reactivity is important to the mitochondrial localisation of **2** and **29**. It is reasonable that cationic, lipophilic species (such as **14**) are taken into mitochondria, due to the potential

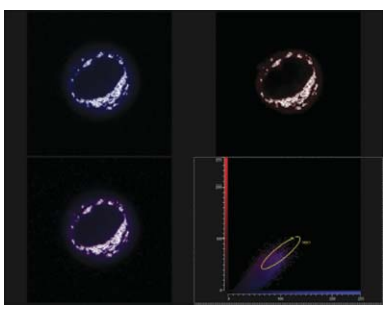

Fig. 15 Colocalisation of **14** and TMRE showing significant overlap.

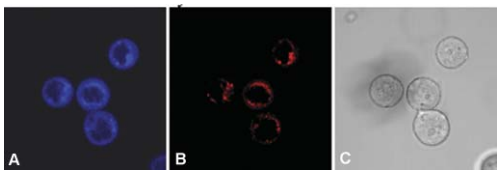

Fig. 16 Fluorescence from Re (A) TMRE (B) and transmitted light (C) images of **14** and TMRE co-administered to MCF-7 cells demonstrating the more diffuse distribution of **14**.

gradient across the mitochondrial membrane, but are also to be found at high concentrations in other lipophilic localities of the cell. It is also known that **29** is a thiol-reactive species which would be expected to be irreversibly concentrated in the mitochondria. The fact that the pattern of distribution of **2**, which would be expected to be *less* lipophilic than **14**, more resembles that of the thiol-reactive species **29** than **14** suggests that it is endowed with some property which 'fixes' it in mitochondria, of which phosphorylation to the thiol-reactive entity seems a likely possibility. Other than in the mitochondria, the non-uniform pattern of distribution of **14** throughout the cytoplasm indicated that the hydrophobic membranes of the endoplasmic reticulum and the Golgi body were targeted. Remarkably, the apparently very closely related simple cyclohexylamine-derived amide **15** was extremely poorly taken up by MCF-7 cells. It was uncertain from confocal microscopy experiments whether *any* uptake had occurred at all. Some extremely faint luminescence was detected from intact cells centred at shorter wavelength than is typical for ^{3}MLCT which was assigned to autofluorescence (Fig. 17). The only intense rhenium-based (*i.e.* centred around 550 nm) luminescence from any cells treated with **15** was seen in that small population of dead or damaged cells found in the sample (Fig. 18). There was no larger proportion of dead or damaged cells in this sample than others, indicating that the association of lumophore followed cell damage, rather than was responsible for it. This association of rhenium complexes with biological constituents of dead and damaged cells, which has been observed for a number of the more lipophilic species, is thought to be a function of physical or simple chemical interactions (*e.g.* hydrophobic interactions) and completely different from (and simpler than) cellular uptake processes. This dramatic difference in uptake

Fig. 17 Overlaid fluorescence and transmitted light images of **15** in MCF-7 cells showing autofluorescence.

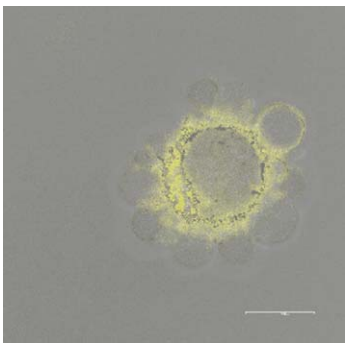

Fig. 18 Overlaid fluorescence and transmitted light images of **15** in MCF-7 cells showing accumulation in dead cells (scale bar = 8 μm).

between such similar complexes **14** and **15** led to a question as to whether this difference in uptake could possibly be rationalised solely in terms of passive diffusion, or whether a more complex explanation must be invoked. In order to clarify this, the simplest possible analogue, **1**, was incubated with MCF-7 and examined by confocal microscopy. Again, as for **15**, uptake was *only* observed for damaged or dead cells and essentially no rhenium-based luminescence was observed in healthy cells. The apparent uptake in dead cells simply reflects the moderate lipophilicity of such species which will associate with organic material in preference to aqueous buffer if they are able to come into contact with material such as lipoprotein membranes. It had been noted that the highly lipophilic species **8–10** were taken up well by dead or damaged cells, whereas the other complexes were only weakly associated with these, and good uptake was seen only in apparently healthy cells. This can be rationalised by proposing that the highly lipophilic species partition so strongly into *e.g.* lipoprotein that they show apparently good uptake whatever the state of the cell, whereas the less lipophilic species show good uptake only if the cells are healthy enough to maintain the potential to provide a healthy cross-membrane gradient which assists the uptake of these cationic complexes. That certain cationic complexes are not taken up when apparently they should be of similar permeability is more surprising. Liposome studies have previously confirmed that species such as **15** are highly membrane-permeable, and it would normally be assumed that the hydroxymethyl group of **2** would render it *more* polar and *less* permeable than **1**. It is therefore difficult to rationalise on grounds of lipophilicity, charge, size or shape why *e.g.* **1** and **2** should differ so markedly in their uptake, and so it is suggested that a difference in the interaction between these species and the glycocalyx layer surrounding the lipid bilayer prevents these complexes from diffusing into the cytoplasm. That small differences in the structures of rhenium complexes have profound effects upon their interactions with the glycocalyx became apparent in experiments involving anionic complexes (*vide infra*).

Anionic complexes

The distribution within cells of anionic complexes **22**, **23** and **28** was studied by incubation with MCF-7 cells followed by confocal microscopy. Interestingly, only the more polar species **22** and **23** showed appreciable association with the cells, while the more lipophilic species **28** showed no evidence of uptake at all. Of the two species which showed cell association, the more polar hydroxylated species **23** showed the better association, while the pattern of localisation was similar. Both species **22** and **23** showed uptake in the outer layers surrounding the plasma membrane region, presumably binding to cationic residues in the peripheral glycoprotein layers (the 'glycocalyx'). The diffuse pattern of localisation can be observed from the Z-stacks of the cells incubated with **23** as a diffuse halo of luminescence surrounding the cell in all dimensions (Fig. 19). A 3D representation of the localisation obtained by recombining the Z-stacks further reveals the diffuse distribution around the exterior perimeter of the cell (Fig. 20). Interestingly, localisation within the pellicular layers is

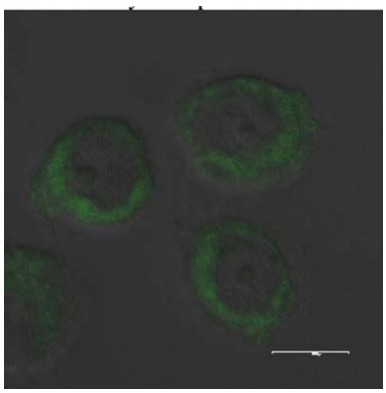

Fig. 19 Overlaid fluorescence and transmitted light images of **23** in MCF-7 cells showing localisation in the exterior plasma membrane (scale bar = 12 μm).

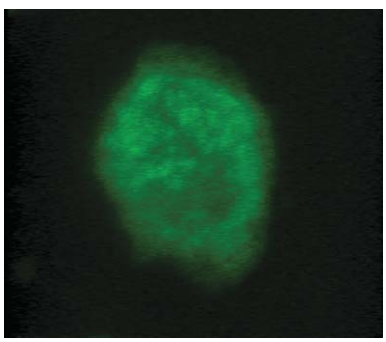

Fig. 20 3D reconstruction showing **23** in the plasma membrane of MCF-7 cell showing diffuse distribution.

clearly non-uniform, with surface patches showing heterogeneous distribution across and within the cellular boundary structure. Both in the image obtained from reconstruction of the Z-scan series and from individual images it is clear that there are hotspots of localisation, the nature of which is yet to be identified.

Conclusions

The localisation and uptake of rhenium lumophores is a complex area, which will require more study to obtain a complete picture; however, certain basic principles are becoming apparent. It appears from this preliminary investigation that cationic species are taken up well by passive diffusion, except for certain cases in which it is proposed that the complex is prevented from entering the lipid bilayer by interaction with the glycocalyx. Highly lipophilic complexes appended with fatty-acid-derived units are taken into dead cells, whereas the other species require a healthy membrane potential to facilitate uptake. Localisation can in many cases be explained in terms of simple chemical processes *e.g.* ionic, hydrophobic, electrostatic hydrogen bonding interactions; however, in some cases the picture is more complex. Simple cationic lipophilic species localise in hydrophobic membranes of the organelles or other cytoplasmic structures, while those which are electrophilic, or can be rendered electrophilic by phosphorylation, localise in the mitochondria. Anionic polar species associate with particular, as yet unidentified, layers associated with the outer face of the plasma membrane, while anionic lipophilic species show little or no uptake. There appears to be little intrinsic toxicity associated with the rhenium tricarbonyl bisimine pyridine unit over the duration of the observation as judged by little deterioration of ultrastructure observable by optical microscopy. Very little photobleaching was observed under the conditions employed in mammalian cells whereas some was observed in yeast cells, albeit still less than expected for an organic fluorophore.

Experimental

Cell culture and imaging

Yeast cell incubation. *Saccharomyces cerevisiae* IFO 0233 or *Schizosaccharomyces pombe* 972h$^-$ cells were harvested by centrifugation (1000 g, 3 min), then washed twice in phosphate buffer saline (PBS, pH 7.4), before resuspension in PBS, incubated with lumophores (final concentration 100 μg ml^{-1}) for 30 min in 0.3% yeast extract, 1% peptone and 1% glucose, rinsed in PBS (×3) and mounted on a slide. Preparations were viewed using a Leica TCS SP2 AOBS confocal scanning laser microscope using a ×63 or ×100 objective, with excitation at 405 nm and detection at 520–570 nm.

Human cell incubation. Human adenocarcinoma cells (MCF-7), obtained from the European Collection of Cell Cultures, Porton Down, Wiltshire, UK, were maintained in Hepes modified minimum essential medium (HMEM) supplemented with 10% foetal bovine serum, penicillin and streptomycin. Cells were detached from the plastic flask using trypsin–EDTA solution, and suspended in an excess volume of growth medium. The homogenous cell suspension was then distributed into 1 ml aliquots with each aliquot being subject to incubation with a different lumophore, final concentration 100 μg ml^{-1}, at 4 °C for 30 min. Cells were finally washed three times in phosphate buffer saline (PBS, pH 7.2), harvested by centrifugation (5 min, 800 g) and mounted on a slide for imaging. Preparations were viewed using a Leica TCS SP2 AOBS confocal laser microscope using ×63 or ×100 objective, with excitation at 405 nm and detection at 520–570 nm.

Co-localisation experiments. MCF-7 adenocarcinoma cells were harvested as indicated above, resuspended in HMEM and incubated with both TMRE (final concentration 100 nM) and rhenium complexes (final concentration 20 μg ml^{-1}) for 1.5 h at room temperature, before being washed three times in PBS, mounted and viewed as above by confocal microscopy. Images were recorded in each case with excitation at either 405 or 543 nm and detection between 500–600 nm.

Chemical synthesis

General considerations. All starting materials, reagents and solvents were purchased from commercial suppliers and used as supplied unless otherwise stated. ^{1}H-NMR and ^{13}C-NMR spectra were recorded at 400 and 100 MHz, respectively, on a Bruker DPX and referenced to residual solvent peaks unless otherwise reported. IR spectra were recorded on a Perkin Elmer 1600 FT IR as thin films or nujol mulls and are reported in wavenumbers. Mass spectra were recorded on a VG Fisons Platform II or at the EPSRC national mass spectrometry service in Swansea (HRMS). Elemental analyses were performed by Warwick Analytical Services (University of Warwick). All photophysical data were obtained on a JobinYvon–Horiba Fluorolog spectrometer fitted with a JY TBX picosecond photodetection module and a Hamamatsu R5509-73 detector (cooled to –80 °C using a C9940 housing). Excitation and emission maxima are limited in accuracy to the monochromator slit width of 5 nm. $ReCl(bipy)(CO)_3$[6] $[ReCl(bipy)(CO)_3(CH_3CN)]BF_4$[6] and **4**, **8**, **9**, **19**, **20**, **21**, **22** and **23** were prepared according to the literature[6,10] methods. Numbering for rhenium complexes given in Fig. 21.

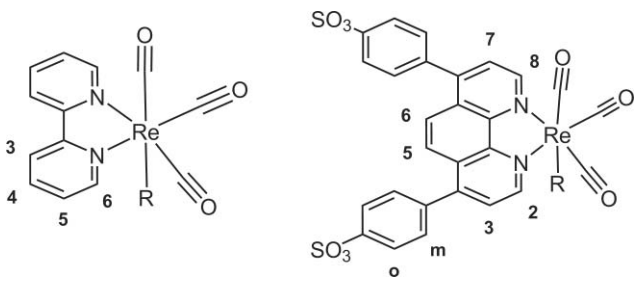

Fig. 21 Numbering for rhenium complexes.

fac-[Re(bipy)(CO)$_3$PyCH$_2$OH][BF$_4$] (2)

$Re(bipy)(CO)_3CH_3CN](BF_4)$[6] (255 mg, 0.4 mmol) and 3-(hydroxymethyl)pyridine (0.45 ml, 4 mmol) were heated at reflux in tetrahydrofuran (175 ml) under a nitrogen atmosphere for 1.5 h. After the solution had cooled, petroleum ether was added dropwise to crystallize the product as a yellow solid (178 mg, 62% yield), m.p. 200 °C. δ_H (CD_3CN) 9.18 (2H, d, J = 5.5 Hz, C*H*(6) bipy), 8.30 (2H, d, J = 8.1 Hz, C*H*(3) bipy), 8.2 (2H, m, C*H*(4)

bipy), 8.12 (1H, s, C*H*(2) Py), 8.04 (1H, d, $J = 5.5$ Hz, C*H*(6) Py), 7.68–7.78 (m, 3H, C*H*(4) Py, C*H*(5) bipy), 7.18 (1H, m, C*H*(5) Py), 4.38 (2H, s, CH_2), 3.33 (1H, s, O*H*). δ_C (CD_3CN) 195.4 ($CO_{eq.}$), 191.3 ($CO_{ap.}$), 155.4 (*C*(3), py), 153.5 (*C*(6), bipy), 150.0 (*C*(6), py), 149.5 (*C*(2), py), 140.8 (*C*(3), bipy), 140.6 (*C*(2), bipy), 137 (*C*(5), py), 127.8 (*C*(4), bipy), 125.8 (*C*(4), py), 124.3 (*C*(5), bipy), 59.6 (*C*H_2). ν_{max} (Nujol) 2032 s, 1915sb υ (CO). *m*/*z* (ESI) 536.1 $[MH]^+$, 427 $[M–BF_4–PyCH_2OH]^+$. Elemental analysis, found C, 36.68; H, 2.30; N, 6.56. $ReC_{19}H_{15}O_4N_3BF_4$ requires C, 36.65; H, 2.41; N, 6.75.

fac-[Re(CO)$_3$(2,2-bipyridine)(cyclohexylnicotinate)][BF$_4$] (14)

[Re(CO)$_3$(2,2-bipy)NCCH$_3$](BF$_4$)[6] (100 mg, 19 mmol) and cyclohexylnicotinate (100 mg, 49 mmol) were dissolved in chloroform (2 ml) and were heated to 60 °C for 12 h, and the product was precipitated with diethyl ether (10 ml) to afford a yellow powder (67 mg, 52%). δ_H (CD_3CN) 9.17 (2H, d, $J = 5.1$ Hz, A), 8.85 (1H, s, H), 8.76 (2H, d, $J = 7.9$ Hz, C), 8.38 (4H, m, D+E+G), 7.82 (2H, t, $J = 7.0$ Hz, B), 7.59 (1H, td, $J = 6.4$ Hz,F), 5.02 (1H, m, I) 1.92 – 1.36 (10H, m, J+K+L); δ_C (CD_3CN) 162.2, 155.8, 155.6, 153.4, 151.4, 141.0, 139.7, 129.3, 128.5, 126.6, 124.5, 74.4, 30.6, 24.9, 22.7. ν_{max} (CH_3CN) 2022 (CO), 1917 (CO), 1635 (COOR). Theoretical isotope pattern 630.12 (58%), 631.12 (17%), 632.12 (100%), 6.33.12 (29%), 634.13 (5%). Observed isotope pattern 630.16 (53%), 631.16 (17%), 632.16 (100%), 633.17 (28%), 634.17 (5%). Crystal data for **14**: $C_{26}H_{12.50}BF_4N_3O_4Re$, $M = 703.90$, yellow needle, $0.20 \times 0.20 \times 0.15$ mm^3, orthorhombic, space group *Pnma*, $a = 16.7420(3)$, $b = 12.4980(4)$, $c = 12.0760(4)$ Å, $V = 2526.80(12)$ Å^3, $Z = 4$, $D_c = 1.850$ g cm^{-3}, $F000 = 1350$, Mo-Kα radiation, $\lambda = 0.71073$ Å, $T = 150(2)$ K, $2\theta_{max} = 55.0°$, 9904 reflections collected, 3019 unique ($R_{int} = 0.0561$). Final *GooF* = 1.341, $R_1 = 0.0474$, w$R_2 = 0.1363$, *R* indices based on 3019 reflections with $I > 2\sigma(I)$ (refinement on F^2), 212 parameters, 0 restraints

fac-[Re(CO)$_3$(2,2-bipyridine)(cyclohexylnicotinamide)][OTf] (15)

[Re(CO)$_3$(2,2-bipyridine)(OTf)] (60 mg, 12 mmol) and cyclohexylnicotinamide (24 mg, 12 mmol) were dissolved in acetonitrile (2 ml). The solution with heated to 60 °C for 12 h and the product was precipitated with diethyl ether (10 ml) to afford a yellow powder (59 mg, 81%). δ_H (CD_3CN) 9.27 (2H, d, $J = 5.1$ Hz, A), 8.51 (1H, d, $J = 1.7$ Hz, E), 7.84 (2H, td, $J = 1.1$ Hz, J′ = 4.5 Hz, B), 7.40 (1H, dd, $J = 5.7$ Hz, J′ = 2.2 Hz, F), 7.10 (1H, d, $J = 7.2$ Hz, I) 3.75 (1H, m, J), 1.73 (5H, m, K), 1.28 (5H, m, L). δ_C (CD_3CN) 195.4 (CO), 161.6 (CONH), 155.5, 153.5, 150.8, 140.9, 137.4, 128.5, 125.9, 124.5, 48.9, 31.8, 24.9, 24.5. ν_{max} (CH_3CN) 2036 (CO *trans* to Py), 1933 (CO), 1635 (CONH). Theoretical isotope pattern 629.13 (61%) 630.14 (22%) 631.14 (100%) 632.14 (32%) 633.14 (11%). Observed isotope pattern 629.14 (36%) 630.15 (11%) 631.13 (100%) 632.14 (27%) 633.13 (81%). Crystal data for **15**: $C_{26}H_{24}F_3N_4O_7Re_S$, $M = 779.75$, $0.20 \times 0.20 \times 0.20$ mm^3, monoclinic, space group *P*21/*c* (No. 14), $a = 12.1380(3)$, $b = 12.1560(3)$, $c = 19.4130(5)$ Å, $\beta = 105.8630(10)°$, $V = 2755.30(12)$ Å^3, $Z = 4$, *D*c = 1.880 g cm^{-3}, $F000 = 1528$, Mo-Kα radiation, $\lambda = 0.71073$ Å, $T = 293(2)$ K, $2\theta_{max} = 61.0°$, 11446 reflections collected, 7278 unique ($R_{int} = 0.0300$). Final *GooF* = 1.071, $R_1 = 0.0373$, w$R^2 = 0.0698$, *R* indices based on 6007 reflections with $I > 2\sigma(I)$ (refinement on *F*2), 379 parameters, 0 restraints. Lp and absorption corrections applied, $\mu = 4.559$ mm^{-1}.

fac-[Re(1,10-bathophenanthroline sulfonate)(CO)$_3$PyCH$_2$OCO(CH$_2$)$_{12}$CH$_3$][H$_4$N] (28)

Mystiric acid (18 mg, 0.08 mmol) was added to a mixture of EDCI (26 mg, 0.1 mmol) and DMAP (4 mg, 0.03 mmol) in dry dichloromethane (5 ml) at 0 °C. After 15 min stirring under a nitrogen atmosphere, a solution of complex **23**[6] (50 mg, 0.04 mmol) in dry DCM (3 ml) was added to the reaction mixture, and stirring was continued at room temperature for 2 h. The solvent was evaporated to dryness and the residue was washed with ethyl acetate to remove the excess EDCI and DMAP. The yellow solid was dissolved in the minimum amount of methanol and it was passed through an ion exchange column (Amberlite IR120 H resin as NH_4^+ form) which had previously been washed with aqueous ammonia eluting with methanol–water (1 : 1). The yellow coloured fraction which eluted immediately was collected, evaporated and dried under vacuum to give **28** as a yellow solid (27 mg, 62%), m.p. 167 °C δ_H (CD_3OD) 9.71 (2H, m C*H*(2,9)), 8.45 (1H, m, C*H*(6′)), 8.32 (1H, s, C*H*(2′)), 8.10 – 7.97 (8H, m, 4 × C*H*(o), C*H*(3,5,6,8)) 7.78 (1H, dd, $J = 1.5$, 7.8 Hz C*H*(4′)), 7.69 – 7.70 (4H, m, 4 × C*H*(m)) 7.25 (1H, t, $J = 7.8$, 5.7 Hz, C*H*(5′)), 4.83 (2H, s, PyCH_2O), 2.03 (2H, t, $J = 7.4$ Hz, C*H*(10′)), 1.25 – 0.85 (22H, m, C*H*(11′21′)), 0.79 (2H, m, CH_3(22)). δ_C (CD_3OD) 197.1 (CO_{eq}), 192.9 (CO_{ap}), 174.9 (*C*O(9)), 154.1, 152.6, 152.5 (2C), 152.2, 147.0, 145.0, 143.7, 140.4, 138.1, 131.9, 130.9, 130.6, 130.3, 129.8, 129.6, 128.1, 127.9, 127.6 (2C), 127.4 (3C), 127.2, 127.1, 126.8 (2C), 126.6, 126.2, 62.6 (Py*C*H_2O), 33.9 (*C*(10)), 32.4 (*C*(11)), 30.0, 29.9 (2C), 29.7 (2C), 29.4, 29.1 (2C), 25.1 (*C*(20)), 23.0 (*C*(21)), 13.7 (*C*(22)). ν_{max} (CH_3CN) 2030, 1826, 1738 (CO); *m*/*z* (ESI) 1080.3 $[MH_2+NH_4]^+$, 761.1 $[MH_2–PyCH_2OCO(CH_2)_{12}CH_3–NH_4]^+$. Theoretical isotope pattern $[M]^-$ 1078.2 (55%), 1079.2 (30%), 1080.2 (100%), 1081.2 (58%), 1082.2 (38%), 1083.2 (6%). Actual isotope pattern $[M]^-$ 1078.4 (42%), 1079.4 (45%), 1080.3 (100%), 1081.3 (60%), 1082.4 (21%), 1083.3 (2%) found C 49.07 H 4.94 N 5.08 $C_{45}H_{51}N_4O_{11}ReS_2 \cdot H_2O$ requires C 49.48 H 4.89 N 5.13%.

fac-[Re(bipy)(CO)$_3$PyCH$_2$Cl][PF$_6$] (29)

A solution of *fac*-[Re(bipy)(CO)$_3$PyCH$_2$OH](BF$_4$) and **2** (150 mg, 0.2 mmol) in thionyl chloride (3 ml) was stirred under a nitrogen atmosphere overnight. The mixture was cooled in an ice bath and a saturated aqueous ammonium hexafluorophosphate solution was added dropwise over 10 min, with extremely rapid stirring until a yellow solid precipitate formed. The precipitate was separated from the mixture of solvents by filtration and washed several times with water to give **29** as a yellow solid (132 mg, 78% yield), m.p. 180 °C. δ_H (CD_3CN) 9.18 (2H, d, $J = 5.4$ Hz, C*H*(6) bipy), 8.42 (2H, d, $J = 6.4$ Hz, C*H*(3) bipy) 8.32 (3H, m, C*H*(2) Py, C*H*(4) bipy), 8.20 (1H, d, $J = 5.5$ Hz, C*H*(6) Py), 7.91 (1H, d, $J = 4.5$ Hz, C*H*(4) Py), 7.82 (2H, m, C*H*(5) bipy), 7.33 (1H, m, C*H*(5) Py), 4.58 (2H, s, CH_2). δ_C (CD_3CN) 195.0 ($CO_{eq.}$), 191.2 ($CO_{ap.}$) 155.2 (*C*(2), bipy), 153.4 (*C*(6), bipy), 151.0, 151.1 (*C*(2), Py, *C*(6), Py), 140.7 (*C*(4), bipy), 139.0 (*C*(4), Py), 136.6 (*C*(3), Py), 128.3 (*C*(3), bipy), 126.1 (*C*(5), Py), 124.2 (2*C*(5), bipy), 41.1 (*C*H_2). ν_{max} (Nujol): 2027, 1922, 1895 (CO). *m*/*z* (ESI) 553.9 $[MH]^+$ and 427.0 $[M–PF_6–PyCH_2Cl]^+$. Theoretical isotope pattern 552.0 (52%), 553.0 (11%), 554.0 (100%), 550.0 (22%), 556.0 (31%) and 557.0 (8%); observed isotope pattern 551.9 (50%), 552.9 (11%),

553.9 (100%), 554.9 (22%), 556.0 (30%) and 557.0 (5%). HRMS (ESI) calculated $[M–PF_6]^+$ = 552.0248; measured $[M–PF_6]^+$ = 552.0252. $ReC_{19}H_{14}O_3N_3ClPF_6$ requires C, 32.65; H, 2.02; N, 6.01; found C, 32.46; H, 1.92; N, 5.93%.

Acknowledgements

We thank the EPSRC for support (EP/D080401/1; EP/H501118/1) and the EPSRC National Mass Spectrometry Service Centre Swansea for assistance with obtaining mass ions on the labile rhenium complexes.

Notes and references

1 (*a*) S. Ishida, J. Lee, D. J. Thiele and I. Herskowitz, *Proc. Natl. Acad. Sci. U. S. A.*, 2002, **99**, 14298; (*b*) A. Younes, J. A. Songadele, J. Maublant, E. Platts, R. Pickett and A. Veyre, *J. Nucl. Cardiol.*, 1995, **2**, 327; (*c*) V. Fernández-Moreira, F. L. Thorp-Greenwood and M. P. Coogan, *Chem. Commun.*, 2010, **46**, 186; (*d*) M. S. Lowry, W. R. Hudson, R. A. Pascal and S. Bernhard, *J. Am. Chem. Soc.*, 2004, **126**, 14129; (*e*) D. J. Stufkens and A. Vlcek, Jr, *Coord. Chem. Rev.*, 1998, **177**, 127; (*f*) A. Juris, V. Balzani, F. Barigellatti, S. Campagna, P. Belser and A. von Zelewsky, *Coord. Chem. Rev.*, 1988, **84**, 85.
2 *Handbook of Biological Confocal Microscopy*, ed. J. B. Pawlet, Springer, New York, 2006.
3 C. A. Puckett and J. K. Barton, *J. Am. Chem. Soc.*, 2007, **129**, 46.
4 K. K.-W. Lo, W.-K. Hui, C.-K. Chung, K. H.-K. Tsang, D. C.-M. Ng, N. Zhu and K.-K. Cheung, *Coord. Chem. Rev.*, 2005, **249**, 1434.
5 (*a*) C. P. Montgomery, B. S. Murray, E. J. New, R. Pal and D. Parker, *Acc. Chem. Res.*, 2009, **42**, 925; (*b*) E. J. New, D. Parker, D. G. Smith and J. W. Walton, *Curr. Opin. Chem. Biol.*, 2010, **14**, 238; (*c*) G-L. Law, R. Pal, L. O. Palsson, D. Parker and K-L. Wong, *Chem. Commun.*, 2009, 7321.
6 A. J. Amoroso, M. P. Coogan, J. E. Dunne, V. Fernández-Moreira, J. B. Hess, A. J. Hayes, D. Lloyd, C. Millet, S. J. A. Pope and C. Williams, *Chem. Commun.*, 2007, 3066.
7 S. James, K. P. Maresca, J. W. Babich, J. F. Valliant, L. Doering and J. Zubieta, *Bioconjugate Chem.*, 2006, **17**, 590.
8 K. K.-W. Lo, M.-W. Louie, K.-S. Sze and J. S.-Y. Lau, *Inorg. Chem.*, 2008, **47**, 602.
9 N. Viola-Villegas, A. E. Rabideau, M. Bartholom, J. Zubieta and R. P. Doyle, *J. Med. Chem.*, 2009, **52**, 5253.
10 A. J. Amoroso, M. P. Coogan, J. E. Dunne, V. Fernández-Moreira, J. B. Hess, A. J. Hayes, D. Lloyd, C. Millet, S. J. A. Pope and C. Williams, *New J. Chem.*, 2008, **32**, 1097.
11 M-W. Louie, H-W. Liu, M. H-C. Lam, T-C. Lau and K. K-W. Lo, *Organometallics*, 2009, **28**, 4297.
12 D. J. Stufkens, A. Vlcek and Jr, *Coord. Chem. Rev.*, 1998, **177**, 127.
13 M. S. Wrighton and D. L. Morse, *J. Am. Chem. Soc.*, 1974, **96**, 998.
14 R. Y. Tsien, *Nature*, 1981, **290**, 527.
15 C. O. Badgett and C. F. Woodward, *J. Am. Chem. Soc.*, 1947, **69**, 2907.
16 B. Singh, *Tetrahedron Lett.*, 1971, **12**, 321.
17 Commercially available, but prepared as in D. Sharma, B. Narasimhan, P. Kumar and A. Jalbout, *Eur. J. Med. Chem.*, 2009, **44**, 1119.
18 I. Costa, M. Montalti, P. Piersandro, A. Perotti, L. Prodi and N. Zaccheroni, *J. Organomet. Chem.*, 2000, **593**, 267.
19 G. M. Sheldrick, *Acta Crystallogr., Sect. A: Found. Crystallogr.*, 2008, **64**, 112.
20 L. J. Farrugia, *J. Appl. Crystallogr.*, 1997, **30**, 565.
21 M. P. Coogan, J. B. Court, V. L. Gray, A. J. Hayes, S. H. Lloyd, C. O. Millet, S. J. A. Pope and D. Lloyd, *Photochem. Photobiol. Sci.*, 2010, **9**, 103.